# Imaging of single-chromophore molecules in aqueous solution near a fused-silica interface

Lloyd M. Davis, Wesley C. Parker, David A. Ball,
Center for Laser Applications, University of Tennessee Space Institute,
411 B.H. Goerthert Parkway, Tullahoma, Tennessee 37388

John G.K. Williams, Greg R. Bashford,
Pamela Sheaff, Robert Eckles, Don T. Lamb and Lyle R. Middendorf,
LI-COR, Inc., Biotechnology Division, P.O. Box 4000, Lincoln, Nebraska 68504

## ABSTRACT

Single molecules of unconjugated Bodipy-Texas Red (BTR), BTR-dimer, and BTR conjugated to cysteine, in aqueous solutions are imaged using total-internal-reflection excitation and through-sample collection of fluorescence onto an intensified CCD camera, or a back-illuminated frame transfer CCD. The sample excitation is provided by the beam from a continuous-wave krypton ion laser, or a synchronously-pumped dye laser, operating at 568 nm. In order to essentially freeze molecular motion due to diffusion and thereby enhance image contrast, the laser beam is first passed through a mechanical shutter, which yields a 3-millisecond laser exposure for each camera frame. The laser beam strikes the fused-silica/sample interface at an angle exceeding the critical angle by about 1 degree. The resultant evanescent wave penetrates into the sample a depth of approximately 0.3 microns. Fluorescence from the thin plane of illumination is then imaged onto the camera by a water immersion apochromat (NA 1.2, WD 0.2 mm). A Raman notch filter blocks Rayleigh and specular laser scatter and a band-pass-filter blocks most Raman light scatter that originates from the solvent. Single molecules that have diffused into the evanescent zone at the time of laser exposure yield near-diffraction-limited Airy disk images with diameters of ~5 pixels. While most molecules diffuse out of the evanescent zone before the next laser exposure, stationary or slowly moving molecules persisting over several frames, and blinking of such molecules, are occasionally observed.

**Keywords:** Single-molecule detection, single-molecule imaging, single-molecule spectroscopy

## 1. SINGLE MOLECULE DETECTION IN SOLUTION

Although this symposium is on multi-photon microscopy and its applications, the experiments reported in this paper use only single-photon induced fluorescence. (The paper was to be presented in a symposium on fluorescence correlation spectroscopy and single molecule methods, to be chaired by R. Rigler and E. Elson, but unfortunately that symposium was canceled and the paper was rescheduled into the present session.) Two-photon excitation has been used for single-molecule detection in solution, as first reported by Webb, *et al*,[1] but high laser irradiances are generally required because of the low two-photon cross-sections. For such experiments, typically a modelocked laser is focused to a diameter of only 1 micron. However, the goal of our work here is to develop technology to simultaneously image many individual molecules freely moving in solution near a surface over a field of view as wide as 50 microns in diameter. If two-photon excitation were to be used, it would require up to a 2500-fold increase in power to yield the same level of irradiance as in prior experiments. However, if second harmonic generation were to occur at the surface, this would provide a means for one-photon excitation of molecules, and may enable single-molecule detection at surfaces with infrared excitation wavelengths at reduced irradiances.[2]

The key requirement for fluorescence detection of single molecules, whether by one-photon excitation, or by two-photon excitation, is the necessity to achieve adequate signal-to-noise. In general, all sources of extraneous light, autofluorescence of lenses and filters, specular scatter from flow-cell boundaries or particulates, Rayleigh scatter from the solvent, and fluorescence from impurities in solution, must be essentially eliminated. When this is done, the remaining background, in the case of SMD in aqueous solution, will be due largely to Raman scatter from the many water molecules that surround the single dye molecule of interest. The main feature in the Raman spectrum of water,[3] as shown in Figure 1, is the O-H stretch mode, beginning at about 3000 wavenumbers. However, this peak does not overlap the fluorescence emission spectrum of the dye, which typically extends over the range shown by the dotted line in Figure 1, and it can be eliminated by suitable choice of the bandpass interference filter.

Multiphoton Microscopy in the Biomedical Sciences, Ammasi Periasamy, Peter T. C. So, Editors,
Proceedings of SPIE Vol. 4262 (2001) © 2001 SPIE · 1605-7422/01/$15.00

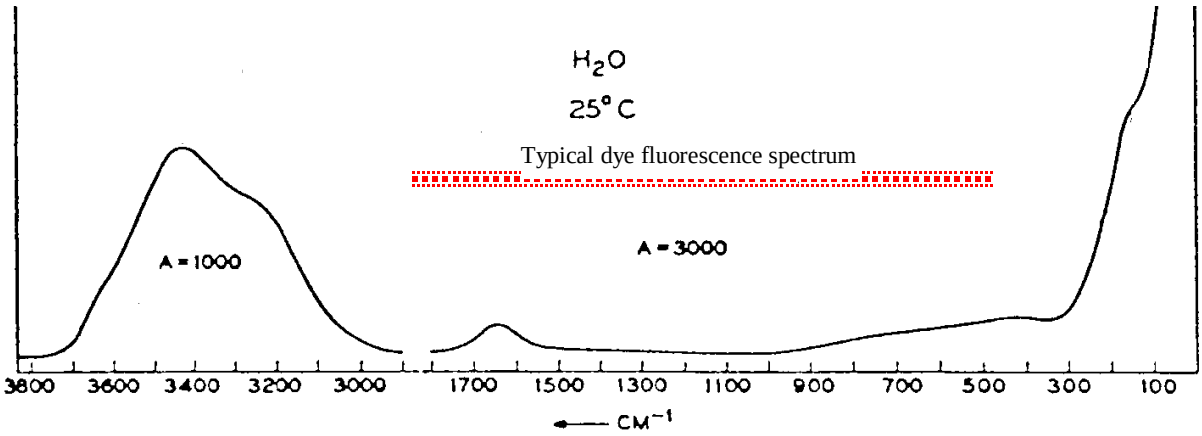


**Figure 1.** Raman spectrum of water

In our single-molecule imaging experiments, for excitation at 568 nm, a 3000—3700 $cm^{-1}$ shift corresponds to a scattered wavelength of 685–720 nm. We use a custom-made interference filter made by Chroma Technology Corporation, Brattleboro, VT, with >80% transmission in the 585–680 nm band, and with optical density >3 in the 690–730 nm band. However, the O-H bend mode, at 1645 $cm^{-1}$, falls within the fluorescence band, at least when visible excitation wavelengths are used, and so it cannot be spectrally discriminated. For a 568 nm excitation wavelength, it falls at 626 nm. The literature value of the differential scattering cross-section for the O-H bend mode is $\approx 10^{-30}$ $cm^2$/Sr/molecule.[4] As the density of water yields $3.34 \times 10^{13}$ molecules/picoliter, the effective total scattering cross-section into $4\pi$ steradians from the O-H bend mode is $\sigma_s \approx 4.2 \times 10^{-16}$ $cm^2$ for 1 picoliter of water. By comparison, the absorption cross-sections of visible dyes are typically somewhat smaller, and fluorescence quantum efficiencies are generally less than unity. By this account, if the laser is to induce more fluorescence signal than Raman O-H bend mode background, the sample volume must be smaller than a fraction of a picoliter. For example, in the case of Texas Red, the absorption cross-section is $\sigma_a \approx 3.7 \times 10^{-16}$ $cm^2$, the fluorescence quantum efficiency is $\Phi_f \approx 0.35$, and the sample volume $V$ must be < 0.3 picoliter for $\sigma_s V < \sigma_a \Phi_f$.

Nevertheless, single molecule detection in solution can be achieved with sample volumes greater than a picoliter by using a modelocked laser and time-gated photon detection to discriminate the Raman O-H bend scatter, as this occurs simultaneously with the laser pulses, whereas fluorescence photons are delayed in time by a mean value equal to the fluorescence lifetime of the dye. In the first report of single-chromophore detection in solution,[5] the sample volume was of the order of 0.9 picoliters and time-gating resulted in a signal-to-noise enhancement by a factor of about 200. In later experiments, a higher efficiency single photon avalanche diode detector[6] was used to build the equivalent of a flow cytometer for single-chromophore molecules.[7] With the addition of a simple gravity-feed flow system and improvements to reduce the dead-time of the time-gating electronics, as shown in Figure 2(a), and by increasing the laser intensity so as to approach the saturation intensity of the dye molecules, rapid counting of single molecules has subsequently been demonstrated.[8] Figure 2(b) shows an example of photon bursts obtained with Texas Red (sulforhodamine 101) using transit times of less than 100 microseconds, as determined from the autocorrelation function of the photon bursts shown in Figure 2(c). The histogram of burst amplitudes is shown in Figure 2(d). With a threshold of 8 photons, the efficiency of single-molecule detection is > 80% and is limited mostly by the modest photostability of the Texas Red in water.

Without time-gating, SMD in solution is most commonly achieved by use of a confocal epi-illumination configuration to restrict the sample volume to a femtoliter or smaller.[9] In this case, the transport of molecules through the probe region is not controlled, but is dominated by diffusion. This is also the case in our experiments on imaging single molecules. Commercial microscope-based systems are now available for fluorescence correlation spectroscopy with single-molecule sensitivity, and design issues have been discussed in other papers within these proceedings. By comparison, in Figure 3(a) is shown a photograph of the system we constructed for single-molecule studies. Instead of a dichroic beam splitter, the unit uses partial reflection from a gimbal-mounted fused silica substrate to introduce the laser beam. The laser beam transmitted by the substrate simply passes to a beam block. Only microwatts of laser power are needed at the sample, the substrate works at any wavelength, and transmission of collected fluorescence by the substrate is greater than 90%. Also noteworthy is the use of a fixed microscope, or an inexpensive CCD camera, to directly view the pinhole for initial alignment of the confocal condition using the back-reflection of the focused laser beam from the coverslip surface.

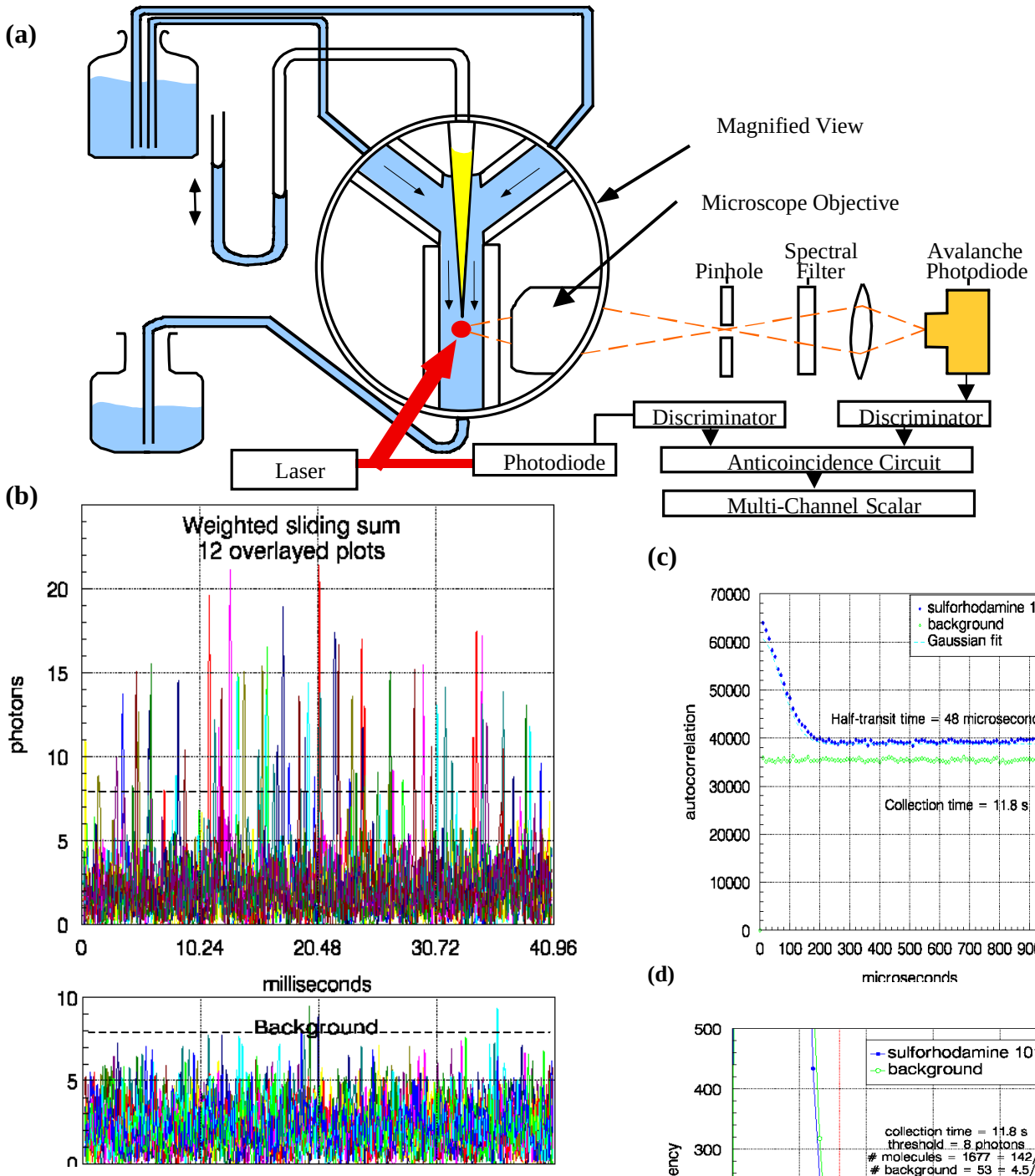


**Figure 2. (a)** Schematic layout of experiment for rapid counting of single-molecules, showing gravity-feed system for sample injection into a sheath flow stream, and electronics for time-gated photon counting. **(b)** Photon bursts obtained when injecting a stream of dilute aqueous sulforhodamine 101 solution, and background obtained when sample injection pressure is removed. **(c)** Autocorrelation functions of photon streams from sample and background. A Gaussian curve fit to the autocorrelation peak yields a half-transit time of 0.48 ms. **(d)** Histogram of burst amplitudes. For a threshold of 8 photons, 1877 and 53 photon bursts are obtained from molecules and background respectively in 11.8 seconds of data.

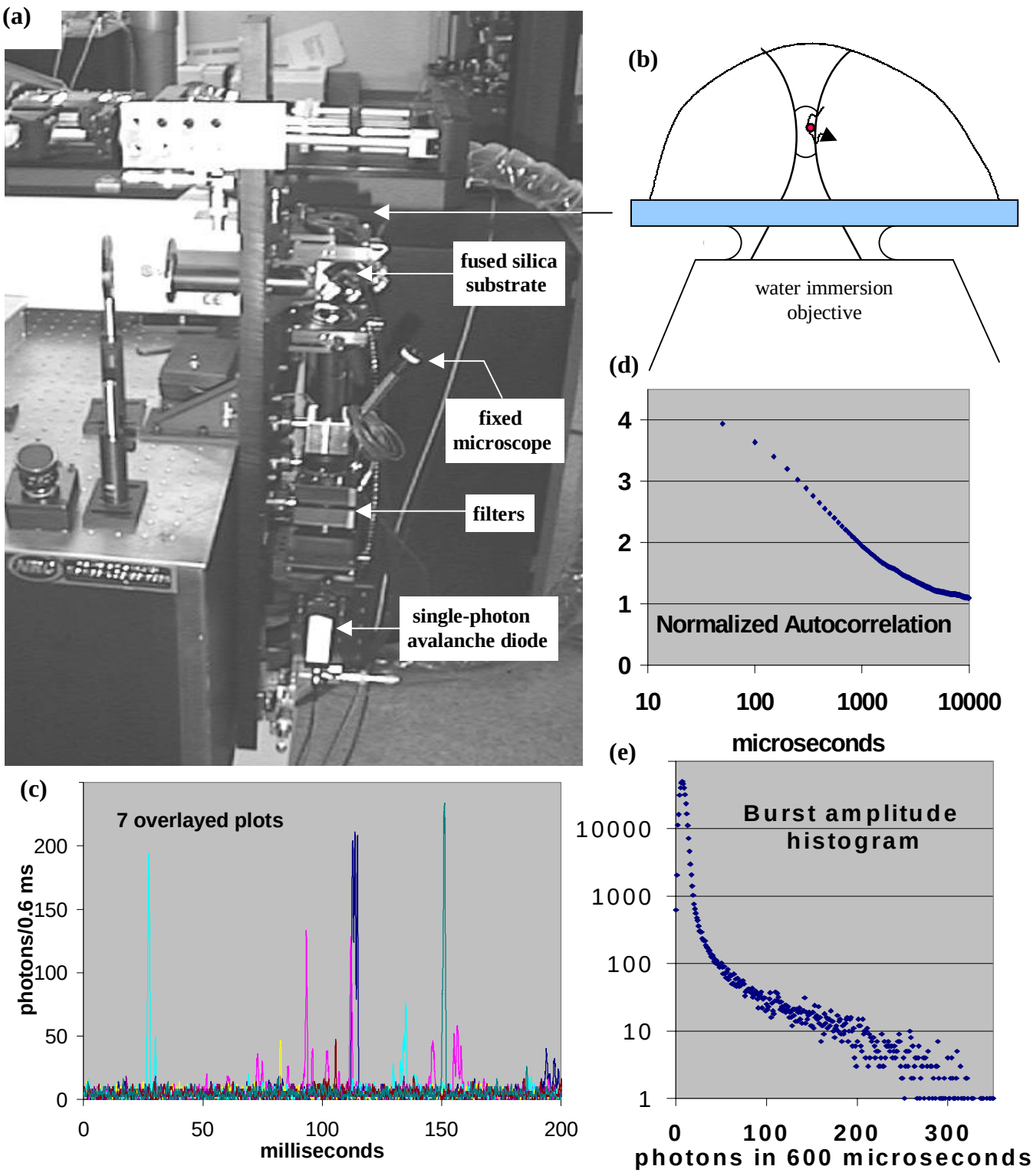


**Figure 3.** **(a)** Photograph of instrument for single-molecule detection by confocal epi-illumination. **(b)** Schematic of water immersion objective, coverslip, and sample drop. **(c)** Example of photon bursts obtained from single molecules of Bodipy Texas Red. **(d)** Normalized autocorrelation function obtained with Bodipy Texas Red. **(e)** Histogram of photon burst amplitudes obtained with Bodipy Texas Red.

Following this initial alignment, the coverslip is then translated down by about 25 microns, so as to avoid collection of coverslip autofluorescence, as shown in the schematic in Figure 3(b). We use a water immersion objective with numerical aperture of 1.2, as this can image deep into a sample without aberration. The sample and coverslip may then be replaced without further alignment. Although oil immersion objectives are available with slightly higher numerical apertures, these are intended to image at the surface of a glass coverslip. The instrument has superb sensitivity and yields single-molecule photon bursts with count rates up to about $5\times10^5$ $s^{-1}$, as shown in Figure 3(c), limited in effect by the dead time of the older-style passively-quenched single-photon avalanche diode detector that it used. TTL pulses from the detector pass to a multichannel scalar card in a PC, and the autocorrelation function, as shown in the example in Figure 3(d), is accumulated by the PC in real time. The width of the autocorrelation function is a measure of the mean diffusional residence time of molecules within the probe region. Figure 3(e) shows an example of the histogram of photon burst amplitudes, in this case collected from a sample of Bodipy Texas Red dye. The instrument has been used for studies of quenching of fluorescence from single molecules, in which the amplitudes of fluorescence bursts from many molecules are measured one by one.

However, certain applications of interest require multiplexed detection of many freely moving single-chromophore molecules simultaneously over a wide field of view, and for this reason, we are now investigating instrumentation for imaging of molecules in solution very near to a surface. As it is necessary to excite and collect light from a region very close to the substrate, autofluorescence of the substrate becomes a key issue. Glass is found to exhibit low-level phosphorescence, and we are currently working with fused silica. This has a refractive index of 1.46, significantly lower than that of glass. In theoretical calculations using Zemax optical design software, and in practice, we find this refractive index difference to result in excessive aberrations if an oil immersion objective is used, even if the coverslip is made very thin. So instead, we are again using a water immersion objective with adjustable coverglass correction collar and slightly lower numerical aperture of 1.2.

## 2. SINGLE MOLECULE IMAGING

There are already many excellent accounts of single molecule imaging in the literature. However, most of these differ from what we are trying to achieve in that the molecules are immobilized or have restricted motion. Betzig, *et al.* first reported near-field imaging of individual molecules on a solid surface with a scanning fiber optic tip.[10] Ishikawa, *et al.*, first reported wide-field imaging of single rhodamine dye molecules evaporated from droplets onto a fused silica substrate using a Hamamatsu intensified silicon-intensified-target (ISIT) camera with single-photon counting capability.[11] Funatsu, *et al.*, reported detection of macromolecules or small molecules in solution labeled by single Cy3 or Cy5 chromophores when these became stationary due to association with an immobilized macromolecule.[12] They used ISIT and intensified CCD cameras, and both epi-illumination and prism-coupled total internal reflection (TIR) excitation in their experiments. Sase, *et al.*, reported the use of a modified epifluorescence microscope to image individual tetramethylrhodamine fluorophores bound to actin filiaments.[13] Schmidt, *et al.*, reported imaging of single labeled lipid molecules in a lipid bilayer.[14] They used epi-illumination with a Gaussian spatial laser profile of 6.1 μm full-width-at-half-maximum and mean intensity of $5.7 \times 10^4$ W $cm^{-2}$. The laser was passed through an acousto-optic modulator to yield 5 ms laser exposures every 35 ms, synchronized to the readout of a $40 \times 40$ pixel CCD region. They measured 2-dimensional diffusion coefficients that were roughly 2 orders of magnitude smaller than that of a small single-chromophore molecule in bulk solution. Dickson, *et al.*, used prism-coupled TIR to image single Nile red molecules in poly(acrylamide) gel and focused attention on about 2 percent of the molecules that moved sufficiently slowly through the evanescent field so as to persist for several seconds.[15] The exponential variation of intensity within the evanescent field results in a position-dependent brightness of fluorescence, which they used to obtain information on the 3-dimensional diffusion. Xu, *et al.*, reported the use of an intensified CCD to image single rhodamine molecules in solution both in prism-coupled TIR mode and in thin layer (4 μm thick) epi-illumination mode.[16] They obtained 1-dimensional streak images with a time resolution of 0.377 ms by operating the CCD in open-shutter mode, and thereby measured diffusion coefficients for rhodamine molecules that were 7 times slower than the bulk solution value, and extended photostabilities. However, the irradiances and solution concentrations quoted in their paper seem to be consistent with those expected for imaging of immobilized entities. A slow down in the diffusion of molecules in micro- or nano-domains has also been observed in confocal epi-illumination single-molecule measurements.[17] Tokunaga, *et al.*, reported the use of prism-less objective-type TIR for imaging single Cy3-labeled ATP molecules when they became associated with an immobilized myosin head molecule.[18] Recently, Ambrose, *et al.*, reported imaging dried rhodamine and surface-immobilized phycoerytherin molecules in solution, with 3 different optical geometries.[19] They found that best signal-to-noise and lowest background was obtained for prism-coupled TIR, as this minimizes excitation of autofluorescence of optical components, but largest signals were obtained with through-substrate collection of fluorescence, because molecules close to a surface emit preferentially into the substrate, at angles above the critical angle.[20] They noted that phycoerytherin molecules that are free in solution and highly mobile diffuse during an integration time and are not imaged as distinct spots.

## 3. EXPERIMENTAL SETUP

Guided by the findings of Ref. 19, and the desire to use larger irradiances in order to image highly mobile molecules, we decided to use the prism-coupled TIR geometry with components made of fused silica to minimize autofluorescence. The refractive index of fused silica is $n_1 = 1.46$, and hence the critical angle is $\theta_c = \sin^{-1}(n_2 / n_1) = 66.02°$, where $n_2 = 1.33$ is the refractive index of water. If a beam of light in a dielectric medium with refractive index $n_1$ is incident upon another dielectric medium with lower refractive index $n_2$ at an angle of incidence $\theta > \theta_c$ then total internal reflection occurs, as shown in Figure 4a.

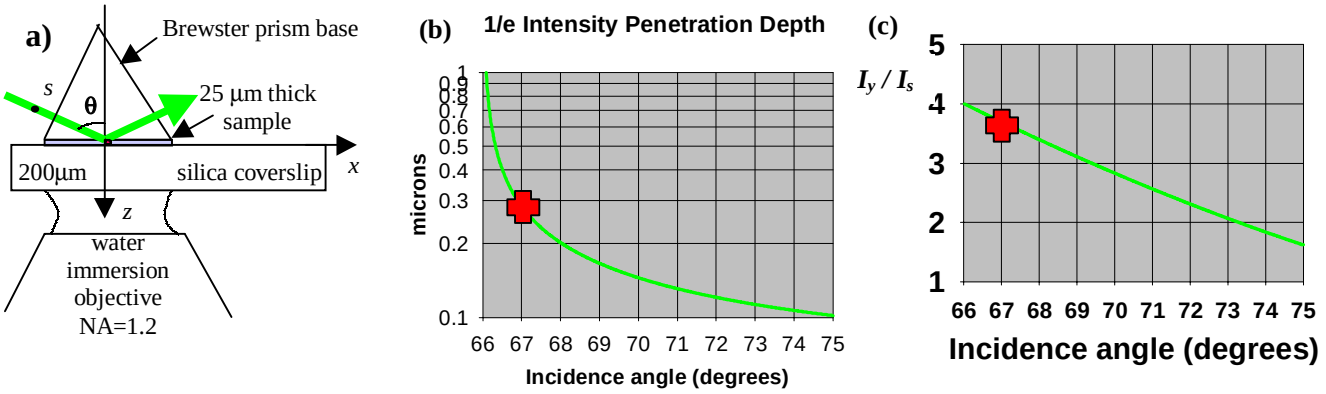


**Figure 4. (a)** Schematic of geometry for prism-coupled total-internal-reflection excitation of a sub-micron layer of solution, as used in our experiments. **(b)** Evanescent field penetration depth versus angle of incidence. **(c)** Evanescent field intensity enhancement factor versus incidence angle for *s*-polarized incident beam.

An evanescent electromagnetic field penetrates into the second medium and the amplitude of the field decays exponentially with distance from the interface:

$$I(z) = I_0 \, e^{-z/d}, \tag{1}$$

where the 1/*e* penetration depth is

$$d = \frac{\lambda_0 / n_2}{4\pi\sqrt{\sin^2\theta - \sin^2\theta_C}}. \tag{2}$$

As seen in Figure 4 (b), for greatest penetration depth, the incidence angle $\theta$ should be close to the critical angle $\theta_c$, but the penetration depth will vary critically with incidence angle.[21] In our experiments, a large penetration depth is desirable in order to increase the residence time of freely diffusing molecules within the evanescent field. Hence the laser beam is focused into the fused silica prism with the beam striking the silica/water interface at a precisely-adjustable angle that is barely above the critical angle. Whereas the phase-fronts at the waist of a focused Gaussian beam are plane, aberrations in the focusing of the beam can yield components with off-axis rays, which would strike the interface below the critical angle and penetrate into the collection optics. In order to minimize coma in the focusing of the beam, the beam should ideally strike the entrance face of the prism at 90°. In our experiments we use a fused silica Brewster prism (Coherent 24-2115), which has an apex angle of $\theta_B = 68.8°$, and a TIR incidence angle of $\theta = 67.0 \pm 0.5°$, as determined trigonometrically using the back-reflection from the entrance face of the prism, yielding a penetration depth of about 0.3 μm. The prism has a high-grade scratch and dig specification of 10-5 (which means that at most 1 dig hole of diameter 50 μm, and smaller dig holes with sum of diameters less than 100 μm, are allowed on the entire prism face).

In the experiments reported in this paper, the incident laser beam polarization is in the *y*-direction, i.e., at right angles to the plane of incidence, and hence the evanescent field is also linearly polarized in the *y*-direction. The total internal reflection of the laser beam from the interface gives rise to a standing wave in the *z*-direction within the prism, and a resultant enhancement in the field at the surface.[21] Within the lower refractive-index water, the intensity is enhanced by a factor of

$$I_y / I_s = \frac{4\cos^2\theta}{1 - (n_2 / n_1)^2}. \tag{3}$$

As shown in Figure 4(c), for an incidence angle of $\theta = 67°$, the enhancement factor is about 3.7.

Figure 5(a) shows a schematic of the optical system used for single-molecule imaging, and Figure 5(b) lists details of the components, as numbered in Figure 5(a). Figure 5(c) is a photograph of the experimental setup, which is built on the frame of a Zeiss Axiovert S100 inverted microscope. The laser beam first enters through a mechanical shutter (labeled in Figure 5(c)), then passes to a periscope, which allows easy adjustment of the position of the beam with respect to the microscope axis, then passes through a focusing achromat lens and into the prism. Figure 5(d) gives a close-up view of the prism. The microscope is bolted to a platform made from Aluminum extrusion, which overhangs the optical table and allows the camera to be directly mounted under the microscope, as shown in Figure 5(e).

Experiments were performed using an intensified Pentamax CCD frame transfer camera, from Roper Scientific, Trenton, NJ. This has a Gen IV photocathode with 46% single photon detection efficiency at 600 nm. The CCD has $512 \times 512$ pixels each of size $15\ \mu m \times 15\ \mu m$, with $1.5\times$ magnification fiber optic coupling to the intensifier, yielding an effective pixel size of $22.5\ \mu m \times 22.5\ \mu m$ and field of view of $11.5\ mm \times 11.5\ mm$. The camera analog-to-digital-converter (ADC) operates at a 5 MHz digitization rate. The frame transfer time is 1.52 ms and the minimum digitization time for a complete frame is 81 ms. The intensifier has adequate gain for single photon detection, but the dynamic range is rather limited and the gain noise is such that the precise number of detected photons cannot be determined.

Roper Scientific also loaned to us for evaluation a Micromax EEV CCD 57 back-illuminated frame transfer CCD, which had 85 % quantum efficiency for light detection at 600 nm. This camera uses a 16-bit ADC, which provides a gain of 1.8 (in order to utilize the 65535 full dynamic range of the ADC over the 120,000 electron full linear well capacity of each CCD single pixel). The pixels are $13.0\ \mu m \times 13.0\ \mu m$ in a $512 \times 512$ format. The readout noise, at 1 MHz digitization, is 8 electrons root-mean-square (rms), which is quite adequate for detecting signals as low as tens of photons per super-pixel. We have successfully imaged single molecules with this camera and we subsequently purchased it for use in our ongoing experiments. A Hamamatsu intensified ISIT camera with modest quantum efficiency was also available.

One problem with the Pentamax intensified CCD is that the intensifier exhibits gain noise and yields a small number of very intense pixels, as shown in Figure 6(a), particularly if low-level background light is present. For an intensifier gain of 100%, a single photon yields ~50 counts upon a dark background of ~25 counts, and hence the intense pixels would correspond to many detected photons. Figure 6(b) shows the existence of tails in the histograms of pixel intensities, which were obtained from 400 image frames under zero or very-low-level incandescent exposure, for camera gain settings of 80%, 90%, and 100%. In principle, such spikes, which occupy one or two adjacent pixels, could be removed by a digital filter, provided that the images of single molecules were larger. This should be the case in our experiments, because at best, the size of the image of a point source is limited by diffraction, and will have an object space diameter of $\delta = 1.22\ \lambda/NA$, where $\lambda$ is the vacuum wavelength of the fluorescence light and NA is the numerical aperture of the microscope objective. Note that the Rayleigh-criterion line-pair resolution, given by $R = \lambda/(2\ NA)$, is smaller and is sometimes quoted in the single-molecule imaging literature. (The latter is often used together with the Nyquist sampling criterion as the basis for determining the optimum microscope magnification for a given numerical aperture and camera pixel size; magnification that yields more than 2 pixels per distance R does not increase the resolution and is said to be "empty".) In our experiment, $\lambda = 610$ nm, NA=1.2, and hence $\delta = 0.62\ \mu m$. For our Zeiss microscope, the magnification is either 63 or $63\times2.5 = 157.5$, yielding image-space Airy disk diameters of 1.7 or 4.3 pixels for the Pentamax camera, or 3.0 or 7.5 pixels for the Micromax CCD. The images we obtain from single molecules indicate that we are close to the diffraction limit. However, very weak molecule images sometimes appear smaller than $\delta$, simply because only a low number of photons have been detected on just one or two pixels. Digital filtering of the images to remove such small features can be expected to result in a decrease in efficiency of single-molecule detection. (Note that in Ref. 16, in which an intensified CCD is used, signals zones from water mostly occupy 1 pixel, which is taken as evidence for the spatial resolution of the system, even though the Airy disk diameter would be 2.6 pixels.)

In order to image molecules that are freely moving due to diffusion in solution, the mechanical shutter that the laser passes through is opened for minimal 3.0 millisecond intervals, as measured with a fast photodiode, in synchrony with the camera. The maximum repetition rate of the shutter is $10\ s^{-1}$ and hence for the Pentamax camera, the interval between successive camera frames is increased from 81 to 100 ms. The shutter provides a series of snapshot images of molecules. For freely diffusing single-chromophore molecules, bulk diffusion coefficients are expected to be about $D = 2.8 \times 10^{-6}\ cm^2\ s^{-1}$ and hence the rms diffusion distance in $t = 3$ ms would be $d = \sqrt{2Dt} = 1.3\ \mu m \approx 2 \times$ Airy diameter $\delta$. Freely diffusing molecules that remain within the evanescent field for the full duration of the exposure would hence give broadened images. However, it would be unlikely for freely diffusing molecules to remain within the 0.3 μm deep evanescent field for the full 3ms exposure. The mean time $t$ that a molecule takes to diffuse a distance $d = 2 \times 0.3\ \mu m$ is $t = d^2/(2D) = 0.64$ ms. Thus the 3 ms duration allows molecules to diffuse in and out of the evanescent field, but is short enough to prevent complete smearing of images.

**(a) Schematic of set up**

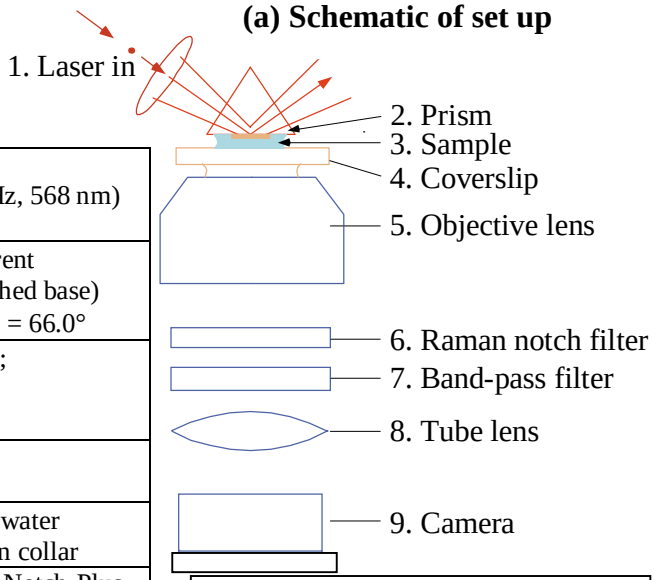


9. Camera: Roper Scientific: Pentamax ICCD frame transfer camera with Gen IV photocathode QE = 46%, 5 MHz ADC

**(b) Components:**

| | | |
|---|---|---|
| 1. | Lasers: | cw Krypton/Argon ion (568 nm);<br>cw modelocked dye (10 ps,76 MHz, 568 nm)<br>s-polarization |
| 2. | Prism: | fused silica, 15mm×15mm (Coherent<br>Brewster prism with custom-polished base)<br>scratch/dig = 10/5 $\theta_B = 68.8° \approx \theta_C = 66.0°$ |
| 3. | Sample: | $6.2 \times 10^{-10}$ M Bodipy-TR in water;<br>2.0 µl drop; 1.0±0.3 cm diameter<br>⇒sample thickness $t \approx 25$ µm |
| 4. | Coverslip: | fused silica, 200 micron thick,<br>SPI Supplies (www.2spi.com) |
| 5. | Objective: | Zeiss 440668 C-Apochromat 63× water<br>immersion NA 1.2, with correction collar |
| 6. | Raman notch filter: | Kaiser Optical holographic Super-Notch-Plus<br>OD>6.0 @568 nm, <350 $cm^{-1}$, 85% T |
| 7. | Band pass filter: | Chroma, 585–680 T>80%, 690–730 OD>3 |
| 8. | Tube lens: | Zeiss; effective focal length 164.5 mm |

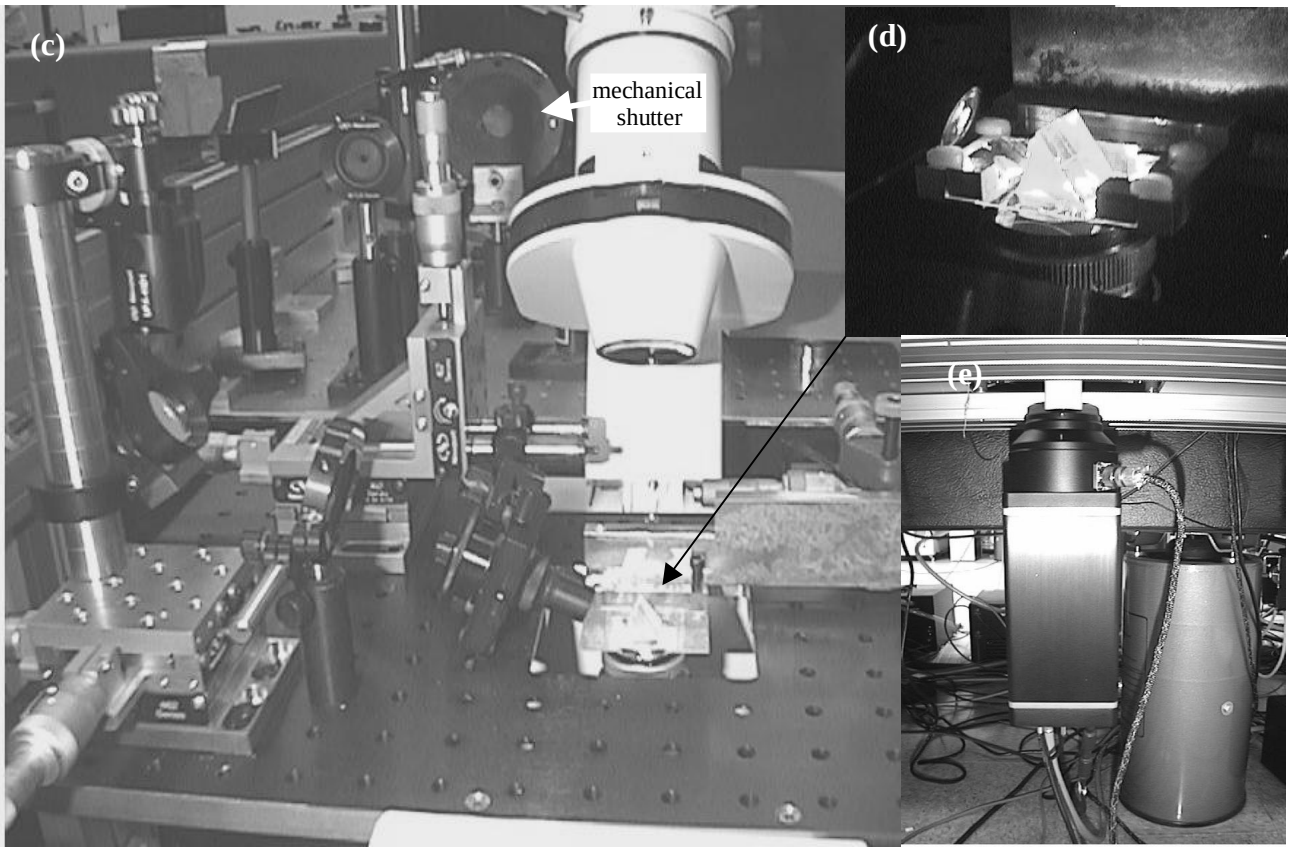


**Figure 5.** Experimental set up for wide-field imaging of molecules with prism-coupled total-internal-reflection excitation **(a)** Schematic of set up. **(b)** Details of components. **(c)** Photograph of experimental set up, built upon a breadboard, mounted on a Zeiss inverted microscope. **(d)** Photograph of prism with laser illumination. **(e)** Photograph of Intensified CCD Camera mounted directly beneath microscope.

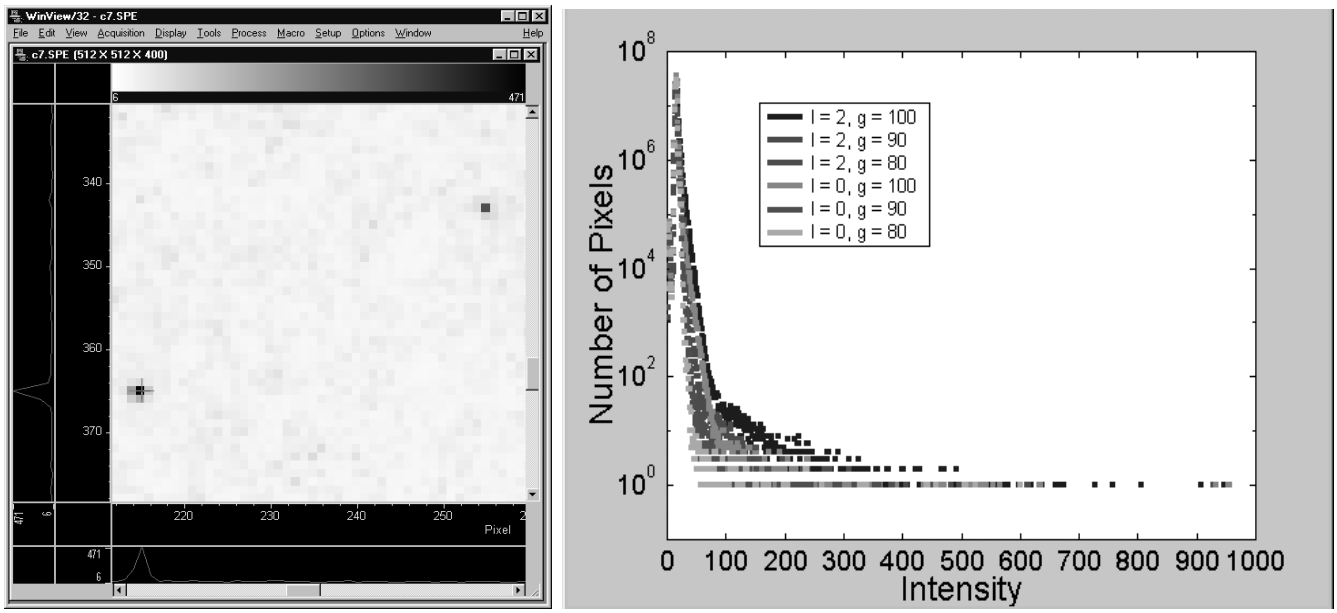


**Figure 6. (a)** Example of a bright pixel within a sub-region of an image obtained with the Pentamax intensified CCD, with low-level incandescent illumination and gain of 80%. The intensity of the bright pixel is considerably higher than that expected from a single photon and corresponds to ~19 photons. **(b)** Histograms of the intensities of individual pixels from 400 frames acquired under intensifier gain settings of 80%, 90%, and 100%, for no illumination (I=0) and for low level incandescent illumination (I=2). The tails in the histograms are due to occasional bright pixels.

## 4. EXPERIMENTAL PROCEDURE, RESULTS AND CONCLUSIONS

In conducting measurements, the prism and coverslip are first cleaned in methanol and then many dilutions of water. The samples are made by serial dilution in water from micro-molar stock solutions. A blank solution is also made by serial dilution of water in water. A 2-microliter drop of the blank solution is first placed onto the fused silica coverslip, then the fused silica prism is placed directly on top. With the weight of the prism, the drop spreads to a diameter of about 1 cm, corresponding to a sample thickness of about 25 μm. Experimental results are to be collected for the blank water sample, but with a clean blank it is difficult to ensure that the microscope is correctly focused. However, when the Raman notch and bandpass filters are removed, specular scatter is visible from surface features, and this is used to focus the microscope. The sample assembly is then translated so as to choose a region with few visible surface features and the filters are replaced. After images are collected from the blank solution, the prism is carefully removed without moving the coverslip and the water is allowed to evaporate. Then a 2-microliter drop of the sample is placed on the coverslip and the prism is again placed on the drop. Some fluorescent molecules are observed on the surface of the prism, and the microscope focus may be adjusted slightly to bring these into best focus.

Experiments have been conducted for a range of laser irradiances and for different samples and sample concentrations. One example of a sequence of subsections of images from unconjugated bodipy Texas Red dye obtained with the pentamax ICCD is shown in Figure 7. For this sequence, the 568 nm laser is focused to a 6 μm × 15 μm ellipse at the prism-sample interface. The mean unchopped laser power is 5 mW, and hence the enhanced intensity at the sample surface is $I_y \approx 2.5 \times 10^4$ W cm$^{-2}$, which is more than a factor of 10 less than the saturation irradiance of the fluorophores. As we step from one image to the next, we see that most molecules appear for just one frame, either because they diffuse out of the evanescent field or photobleach, but some molecules, like those indicated by the open arrows, appear to be stuck to the surface and they fluctuate slightly in position and in brightness, perhaps because of reorientation with respect to the laser polarization. Also noteworthy is a molecule that enters by diffusion and then appears to stick to the surface at the location of the solid arrow in frame 29.

In summary, we note that imaging of freely moving single molecules over a wide field of view is of interest. We have set up an experiment for total-internal-reflection excitation of solution near a fused silica surface. We can easily image surface-adsorbed single-chromophore molecules—these appear to move slightly on the surface consistent with the slower diffusion coefficients seen by others, and sometimes exhibit blinking. By using millisecond pulsed irradiance, we can also image freely moving molecules, which diffuse away or photobleach from one frame to the next.

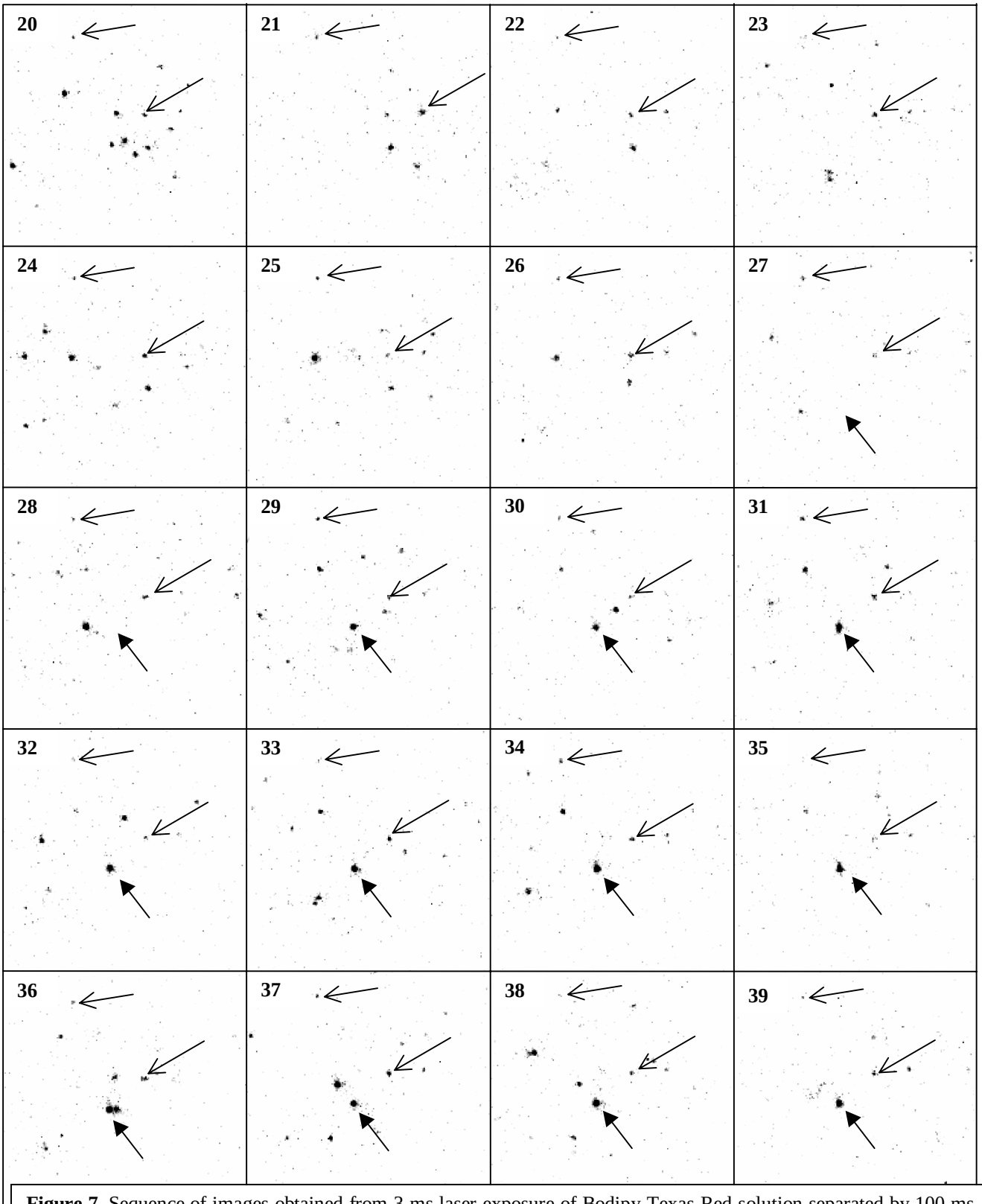


**Figure 7.** Sequence of images obtained from 3-ms laser exposure of Bodipy-Texas Red solution separated by 100 ms, with magnification 157.5. Most detected molecules appear for just a single frame. The molecules indicated by open arrows remain almost stationary but exhibit blinking for the duration of the experiment or until suddenly photobleached. Note the molecule that appears to diffuse into the position of the solid arrow at frame 29, and then stick.

## ACKNOWLEDGEMENTS

We thank Newton Wright for technical support. This work was funded in part by NIH grant 2R44HG02066-02.

## REFERENCES

1. J. Mertz, C. Xu, and W.W. Webb, "Single-molecule detection by two-photon-excited fluorescence," Opt. Lett. **20**, 2532—2534 (1995).
2. J. Enderlein, "New approach to fluorescence spectroscopy of individual molecules on surfaces," Phys. Rev. Lett. **83**, 3804—3807 (1999).
3. G.E. Walrafen, "Raman spectral studies of water structure," J. Chem. Phys. **40**, 3249—3256 (1964).
4. I.I. Kondilenko, P.A. Korotkov, V.A. Klimenko and O.P. Demyanenko, "Transverse cross section of the Raman scattering of the $\nu_1$ vibration of the water molecule in the liquid and gaseous states," Opt. Spectrosc. **43**, 384—386 (1977).
5. E.B. Shera, N.K. Seitzinger, L.M. Davis, R.A. Keller and S.A. Soper, "Detection of single fluorescent molecules," Chem. Phys. Lett. **174**, 553—557 (1990).
6. L.Q. Li and L.M. Davis, "Single photon avalanche diode for single molecule detection," Rev. Sci. Instrum. **64**, 1524—1529 (1993); A. Spinelli, L.M. Davis and H. Dautet, "Actively quenched single-photon avalanche diode for high repetition rate time-gated photon counting," Rev. Sci. Instrum. **67**, 55—61 (1996).
7. L.Q. Li and L.M. Davis, "Rapid and efficient detection of single chromophore molecules in aqueous solution," Appl. Opt. **34**, 3208—3217 (1995).
8. L.M. Davis, "Efficient Counting of Single Molecules with Sub-100 Microsecond Transit Times," South-Eastern Section Meeting of the American Physical Society, Nashville, Tennessee, November 7, 1997.
9. M. Eigen and R. Rigler, "Sorting single molecules: application to diagnostics and evolutionary biotechnology" Proc. Natl. Acad. Sci. USA **91**, 5740—5747 (1991).
10. E. Betzig and R.J. Chichester, "Single molecules observed by near-field scanning microscopy," Science **262**, 1422—1425 (1993).
11. M. Ishikawa, K. Hirano, T. Hayakawa, S. Hosoi and S. Brenner, "Single-molecule detection by laser-induced fluorescence technique with a position-sensitive photon-counting apparatus," Jpn. J. Appl. Phys. **33**, 1571—1576 (1994).
12. T. Funatsu, Y. Harada, M. Tokunaga, K. Saito and T. Yanagida, "Imaging of single fluorescent molecules and individual ATP turnovers by single myosin molecules in aqueous solution," Nature **374**, 555-559 (1995).
13. I. Sase, H. Miyata, J.E.T. Corrie, J.S. Craik and K.Kinosita, Jr., "Real time imaging of single fluorophores on moving actin with an epifluorescence microscope," Biophys. J. **69**, 323—328 (1995).
14. Th. Schmidt, G.J. Schutz, W. Baumgartner, H.J. Gruber, and H. Schindler, "Imaging of single molecule diffusion," Proc. Natl. Acad. Sci. USA **93**, 2926-2929 (1996).
15. R.M. Dickson, D.J. Norris, Y.L. Tzeng and W.E. Moerner, "Three-dimensional imaging of single molecules solvated in pores of poly(alrylamide) gels," Science **274**, 966—969 (1996).
16. X.H. Xu and E.S. Yeung, "Direct measurement of single-molecule diffusion and photodecomposition in free solution," Science **275** 1106—1109 (1997).
17. W.A. Lyon and S. Nie, "Confinement and detection of single molecules in submicrometer channels," Anal. Chem. **69**, 3400—3405 (1997).
18. M. Tokunaga, K. Kitamura, K. Saito, A.H. Iwane, and T. Yanagida, "Single molecule imaging of fluorophores and enzymatic reactions achieved by objective-type total internal reflection fluorescence microscopy," Biochem. Biophys. Res. Comm. **235** 47-53 (1997).
19. W.P. Ambrose, P.M. Goodwin and J.P. Nolan, "Single molecule detection with total internal reflection excitation: Comparing signal-to-background and total signals in different geometries," Cytometry **36** 224—231 (1999).
20. J. Enderlein, "Fluorescence detection of single molecules near a solution/glass interface—an electrodynamic analysis," Chem. Phys. Lett. **308** 263—266 (1999).
21. D. Axelrod, "Total internal reflection fluorescence microscopy," Methods in Cell Biology **30** 245—416 (1989); D. Axelrod, "Total internal reflection fluorescence at biological surfaces," Non-invasive techniques in Cell Biology 94—127 (1990); L.K. Tamm, "Total internal reflectance fluorescence microscopy," p. 295—337 in *Optical Microscopy: Emerging Methods and Applications* Ed. by B. Herman and J.J. Lemasters, Academic Press, San Diego 1993.